2021

Theoretical Analysis of Rigid-Body Vibration in Swing Compressors

Daiki Kikutake
DAIKIN Industries, LTD., Japan, daiki.kikutake@daikin.co.jp

Tatsuya Katayama

Hideki Matsuura

Theoretical Analysis of Rigid-Body Vibration in Swing Compressors

Daiki Kikutake*, Tatsuya Katayama, Hideki Matsuura

Technology and Innovation Center, Daikin Industries, Ltd.,
1-1, Nishi-Hitotsuya, Settsu, Osaka, Japan
Phone: +81-6-6195-7074,
E-mail: daiki.kikutake@daikin.co.jp (Daiki Kikutake),
tatsuya.katayama@daikin.co.jp (Tatsuya Katayama),
hideki.matsuura@daikin.co.jp (Hideki Matsuura)

* Corresponding Author

ABSTRACT

This study aims to theoretically analyze the rigid-body vibration in swing compressors. Currently, low noise and vibration (NV) are qualities recognized as a desired value for an air conditioner by end users. Because the compressor is one of the main sources of NV in an air conditioner, low NV compressors are needed. Designing a low NV compressor requires the understanding of the physical phenomena occurring in a compressor that contribute to NV. In this study, we theoretically analyzed rigid-body vibration, which has been one of the main phenomena causing NV in a swing compressor. Main factors causing rigid-body vibration in the swing compressor were classified into three types of excitation forces. By formulating them in a Fourier series representation, the primary and secondary components in the frequency domain were calculated for each excitation force without any numerical calculation method, including FFT. Furthermore, by multiplying the mass and inertial tensor of the compressor to this, we calculated both the amplitude and phase of the rigid-body vibration generated by each excitation force. We then confirmed that the calculated vibration was consistent with the experimental results. The contribution of each excitation force to the radial and tangential vibrations of typical swing compressors was theoretically analyzed. The results of the analysis clearly indicated that vibration was effectively reduced by not only simply reducing the magnitudes of the excitation forces but also by balancing the excitation forces.

1. INTRODUCTION

Low noise and vibration (NV) are qualities recognized as a desired value for an air conditioner by end users. Low NV of an air conditioner is very important for reliability and user comfort. A compressor is one of the main sources of NV in an air conditioner. Therefore, for an air conditioner to provide high comfort and reliability, a compressor with low NV is required.

NV of a compressor arise from various phenomena that occur in the compressor. Designing a low NV compressor requires a theoretical understanding of the physical phenomena occurring in the compressor that contribute to NV. This theoretical understanding of the phenomena enables us to predict and analyze compressor NV and is very useful for the effective design of a low NV compressor before trial production, troubleshooting of compressors with large NV, and developing new techniques for a low NV compressor.

Rigid-body vibration of a compressor is one of the main phenomena causing NV of an air conditioner. Rigid-body vibration of the compressor, especially the primary and secondary components in the frequency domain, causes sound to not only be radiated from the compressor but also causes high stress for pipes and solid-borne sound to the outdoor unit. Therefore, it is very important to understand the mechanism of the rigid-body vibration of the compressor and to reduce that vibration. As for rotary compressors, which are mainly used in domestic air conditioners, some types of excitation forces are known to cause rigid-body vibration (Imaichi et al., 1982). In order to design a low NV rotary compressor, all the excitation forces should be considered, and the manner by which each excitation force affects the rigid-body vibration of the compressor must be understood.

In this study, we conducted a theoretical analysis of rigid-body vibration for a swing compressor, which is a rotary-type compressor developed by Daikin Industries, Ltd. Firstly, we formulated the rigid-body vibration of a swing compressor. The main factors causing rigid-body vibration in a swing compressor were classified into three types of excitation forces and, by formulation in a Fourier series representation, we obtained the primary and secondary components in the frequency domain without any numerical calculation method, including FFT. Furthermore, by multiplying the mass and inertial tensor of the compressor to this, both amplitude and phase were formulated for the rigid-body vibration generated by each excitation force. Secondly, we measured the rigid-body vibrations of several typical swing compressors, including both single-cylinder type and twin-cylinder type. The calculated vibrations were confirmed to be consistent with the measured ones. Thirdly, for the rigid-body vibrations of each single-cylinder and twin-cylinder compressor, we conducted a theoretical analysis on the contribution of each excitation force to the radial and the tangential vibrations for the primary and secondary components in the frequency domain.

2. THEORY

In this section, we present theoretical equations of rigid-body vibration of a swing compressor. This study classified the main factors causing rigid-body vibration in a swing compressor into three types of excitation forces: centrifugal force of the rotor system, inertial force of the piston, and torque which is generated when refrigerant is compressed. In subsection 2.1, based on an equation of motion for a rigid body, we formulate an arbitrary frequency order for components in the frequency domain for vibration caused by an excitation force. In subsections 2.2 – 2.4, the excitation forces are formulated in a Fourier series representation.

2.1 Equation of Motion for Rigid-Body Vibration

A motion of a rigid body is composed of translational and rotational motions having 3 degrees of freedom, respectively. An equation of motion for a rigid body is expressed as

$$m\ddot{\boldsymbol{r}} + C_r\dot{\boldsymbol{r}} + K_r\boldsymbol{r} = \boldsymbol{F},\ I\ddot{\boldsymbol{\Theta}} + C_\Theta\dot{\boldsymbol{\Theta}} + K_\Theta\boldsymbol{\Theta} = \boldsymbol{T}, \tag{1}$$

where $\boldsymbol{r} = (x, y, z)^{\mathrm{T}}$, $\boldsymbol{\Theta} = \left(\Theta_x, \Theta_y, \Theta_z\right)^{\mathrm{T}}$, $\boldsymbol{F} = \left(F_x, F_y, F_z\right)^{\mathrm{T}}$, $\boldsymbol{T} = \left(T_x, T_y, T_z\right)^{\mathrm{T}}$, m, I, $C_{r,\Theta}$, $K_{r,\Theta}$, are the translational displacement, the rotational displacement, the force, the torque, the mass, the inertial tensor, viscosity matrix, and stiffness matrix, respectively. As for the rigid-body vibration of a compressor, $C_{r,\Theta}$ and $K_{r,\Theta}$ represent the influence of pipes and supporting foot rubbers. This study ignores the influence of the pipes and the rubbers to analyze the compressor's inherent vibration:

$$m\ddot{\boldsymbol{r}} = \boldsymbol{F},\ I\ddot{\boldsymbol{\Theta}} = \boldsymbol{T}. \tag{2}$$

When the rotational speed of the compressor is N, the excitation forces of the vibration become a periodic function with the period of $1/N$. Therefore, $\boldsymbol{F}$ and $\boldsymbol{T}$ are expressed in a Fourier series representation with a fundamental angular frequency of $\omega = 2\pi N$:

$$\begin{aligned}\boldsymbol{F} &= \boldsymbol{F}_0 + \textstyle\sum_j \left(F_{jx}\cos\left(j\omega t + \phi_{F_{jx}}\right), F_{jy}\cos\left(j\omega t + \phi_{F_{jy}}\right), F_{jz}\cos\left(j\omega t + \phi_{F_{jz}}\right)\right)^{\mathrm{T}},\\ \boldsymbol{T} &= \boldsymbol{T}_0 + \textstyle\sum_j \left(T_{jx}\cos\left(j\omega t + \phi_{T_{jx}}\right), T_{jy}\cos\left(j\omega t + \phi_{T_{jy}}\right), T_{jz}\cos\left(j\omega t + \phi_{T_{jz}}\right)\right)^{\mathrm{T}},\end{aligned} \tag{3}$$

where $\boldsymbol{F}_j = \left(F_{jx}, F_{jy}, F_{jz}\right)^{\mathrm{T}}$, $\boldsymbol{\phi}_{F_j} = \left(\phi_{F_{jx}}, \phi_{F_{jy}}, \phi_{F_{jz}}\right)^{\mathrm{T}}$, $\boldsymbol{T}_j = \left(T_{jx}, T_{jy}, T_{jz}\right)^{\mathrm{T}}$, $\boldsymbol{\phi}_{T_j} = \left(\phi_{T_{jx}}, \phi_{T_{jy}}, \phi_{T_{jz}}\right)^{\mathrm{T}}$ are the *j*th component in the frequency domain of the amplitude and the phase of the force and the torque. With Equations (2) and (3), *j*th components in the frequency domain of the translational and rotational vibration acceleration (*jn* translational and rotational vibration) in the compressor are expressed as

$$\ddot{\boldsymbol{r}}_j = m^{-1}\left(F_{jx}\cos\left(j\omega t+\phi_{F_{jx}}\right), F_{jy}\cos\left(j\omega t+\phi_{F_{jy}}\right), F_{jz}\cos\left(j\omega t+\phi_{F_{jz}}\right)\right)^{\mathrm{T}},$$
$$\ddot{\boldsymbol{\theta}}_j = I^{-1}\left(T_{jx}\cos\left(j\omega t+\phi_{T_{jx}}\right), T_{jy}\cos\left(j\omega t+\phi_{T_{jy}}\right), T_{jz}\cos\left(j\omega t+\phi_{T_{jz}}\right)\right)^{\mathrm{T}}. \quad (4)$$

When you want to calculate the *jn* translational vibration at a position $\boldsymbol{R} = (X, Y, Z)^{\mathrm{T}}$ on the compressor $\boldsymbol{a}(\boldsymbol{R})_j$, it is calculated with $\ddot{\boldsymbol{r}}_j$ and $\ddot{\boldsymbol{\theta}}_j$ as

$$\boldsymbol{a}(\boldsymbol{R})_j = \ddot{\boldsymbol{r}}_j + \ddot{\boldsymbol{\theta}}_j \times \boldsymbol{R}. \quad (5)$$

Rigid-body vibration of a compressor has multiple excitation forces. Total *jn* vibration of the compressor is expressed as the sum of the vibration caused by each excitation force:

$$\ddot{\boldsymbol{r}}_{j\mathrm{total}} = \sum_{\mathrm{force}} \ddot{\boldsymbol{r}}_j,\ \ddot{\boldsymbol{\theta}}_{j\mathrm{total}} = \sum_{\mathrm{force}} \ddot{\boldsymbol{\theta}}_j,\ \boldsymbol{a}(\boldsymbol{R})_{j\mathrm{total}} = \sum_{\mathrm{force}} \boldsymbol{a}(\boldsymbol{R})_j. \quad (6)$$

This means that if each excitation force is formulated in a Fourier series representation, we can obtain the contribution of the excitation force to the *jn* vibration separately.

In this study, two types of orthogonal coordinates are defined as shown in Fig. 1. The x, y, z coordinate, which is shown in Fig. 1 (a), has its origin at the center of the cylindrical casing. The z axis coincides with the central axis of the casing and the x axis passes through the central axis of the accumulator. The $x_{\mathrm{cyl}}, y_{\mathrm{cyl}}, z_{\mathrm{cyl}}$ coordinate, which is shown in Fig. 1 (b), has its origin at the center of the cylinder. The z_{cyl} axis coincides with the central axis of the crankshaft (and also with the z axis) and the y_{cyl} axis passes through the center of the swing bushes.

For each excitation force, $\boldsymbol{F} = \left(F_x, F_y, F_z\right)^{\mathrm{T}}$ and $\boldsymbol{T} = \left(T_x, T_y, T_z\right)^{\mathrm{T}}$ are formulated as the following procedure:

1. Formulate $\boldsymbol{F}_{\mathrm{cyl}} = \left(F_{x_{\mathrm{cyl}}}, F_{y_{\mathrm{cyl}}}, F_{z_{\mathrm{cyl}}}\right)^{\mathrm{T}}$ on the $x_{\mathrm{cyl}}, y_{\mathrm{cyl}}, z_{\mathrm{cyl}}$ coordinate in a Fourier series representation
2. Formulate $\boldsymbol{F} = \left(F_x, F_y, F_z\right)^{\mathrm{T}}$ on the x, y, z coordinate by using the following equation:

$$\begin{pmatrix} F_x \\ F_y \\ F_z \end{pmatrix} = \begin{pmatrix} \sin\theta_{\mathrm{suc}} & \cos\theta_{\mathrm{suc}} & 0 \\ -\cos\theta_{\mathrm{suc}} & \sin\theta_{\mathrm{suc}} & 0 \\ 0 & 0 & 1 \end{pmatrix} \begin{pmatrix} F_{x_{\mathrm{cyl}}} \\ F_{y_{\mathrm{cyl}}} \\ F_{z_{\mathrm{cyl}}} \end{pmatrix} \quad (7)$$

3. Formulate $\boldsymbol{T} = \left(T_x, T_y, T_z\right)^{\mathrm{T}}$ on the x, y, z coordinate by using the following equation:

$$\boldsymbol{T} = \boldsymbol{r} \times \boldsymbol{F}, \quad (8)$$

where $\boldsymbol{r} = (x, y, z)^{\mathrm{T}}$ is the position at which $\boldsymbol{F} = \left(F_x, F_y, F_z\right)^{\mathrm{T}}$ applies

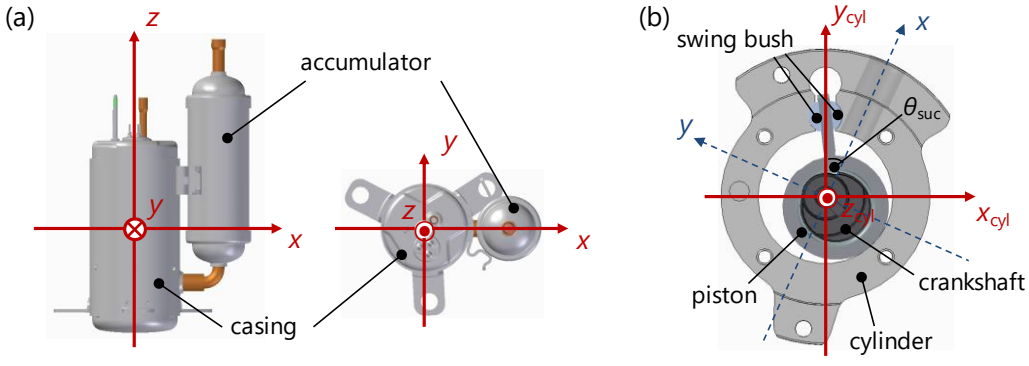

Figure 1: Orthogonal coordinates. (a) x, y, z coordinate. (b) $x_{\mathrm{cyl}}, y_{\mathrm{cyl}}, z_{\mathrm{cyl}}$ coordinate.

2.2 Centrifugal Force of the Rotor System

We define a system composed of a crankshaft, a motor rotor, and balancers attached on the motor rotor as the rotor system, as shown in Fig. 2 (a). When the centrifugal forces applied to the eccentric parts of the system are unbalanced, the unbalanced force excites the vibration of the compressor via its bearings. The balancers are usually designed so that the centrifugal force of the rotor system and the centrifugal force applied to the cylindrical part of the piston are balanced. However, in the usual design of the balancers, the influence of the deflection of the crankshaft is not often considered. As shown in some previous studies (Huang *et al*., 2010 and Zhang *et al*., 2014), the influence of the deflection of the crankshaft on the centrifugal forces is not negligible. Therefore, the deflection of the crankshaft should be calculated at the same time when the centrifugal forces are calculated. The deflection was calculated with a finite element model (FE model) in the previous studies, but this method requires a detailed FE model and takes much calculation time. In this subsection, we formulate the deflection of the crankshaft with a beam deflection based on a material mechanics, and then obtain the unbalanced centrifugal force including the influence of the deflection.

The rotor system was modeled as a beam supported at the upper end of the main bearing (bearing 1) and the lower end of the sub-bearing (bearing 2), as shown in Fig. 2 (b). When the centrifugal forces applied to the upper balancer, the lower balancer, and the motor rotor are denoted as F_{ubw}, F_{lbw}, F_{ro}, respectively, and the deflections of the crankshaft at their respective positions as y_{ubw}, y_{lbw}, y_{ro}, $\boldsymbol{y} = (y_{\mathrm{ubw}}, y_{\mathrm{lbw}}, y_{\mathrm{ro}})^{\mathrm{T}}$ is expressed with $\boldsymbol{F}_{\mathrm{cent}} = (F_{\mathrm{ubw}}, F_{\mathrm{lbw}}, F_{\mathrm{ro}})^{\mathrm{T}}$ as

$$\boldsymbol{y} = A_1 \boldsymbol{F}_{\mathrm{cent}}, \tag{9}$$

where A_1 is influence coefficient matrix. Also, $\boldsymbol{F}_{\mathrm{cent}}$ is expressed with $\boldsymbol{y}$ as

$$\begin{aligned} \boldsymbol{F}_{\mathrm{cent}} &= (m_{\mathrm{ubw}}(y_{\mathrm{ubw}} + r_{\mathrm{ubw}})\omega^2, m_{\mathrm{lbw}}(y_{\mathrm{lbw}} - r_{\mathrm{lbw}})\omega^2, m_{\mathrm{ro}} y_{\mathrm{ro}}\omega^2)^{\mathrm{T}} \\ &= \mathrm{diag}(m_{\mathrm{ubw}}\omega^2, m_{\mathrm{lbw}}\omega^2, m_{\mathrm{ro}}\omega^2)\boldsymbol{y} + (m_{\mathrm{ubw}} r_{\mathrm{ubw}}\omega^2, -m_{\mathrm{lbw}} r_{\mathrm{lbw}}\omega^2, 0)^{\mathrm{T}} \\ &\equiv A_2 \boldsymbol{y} + \boldsymbol{b}_1 \end{aligned} \tag{10}$$

From Equation (9) and (10), $\boldsymbol{y}$ and $\boldsymbol{F}_{\mathrm{cent}}$ are obtained as follows:

$$\boldsymbol{y} = -(A_1 A_2 - I_3)^{-1} A_1 \boldsymbol{b}_1, \boldsymbol{F}_{\mathrm{cent}} = [I_3 - A_2(A_1 A_2 - I_3)^{-1} A_1]\boldsymbol{b}_1, \tag{11}$$

where I_3 is a unit matrix.

As for a single-cylinder type swing compressor, the forces which the rotor system receives from the bearings F_{bear1} and F_{bear2} satisfy following equilibrium equations:

$$F_{\mathrm{bear1}} + F_{\mathrm{bear2}} = F_{\mathrm{ubw}} + F_{\mathrm{ro}} + F_{\mathrm{lbw}} + F_{\mathrm{ecc}}, \tag{12}$$

$$F_{\mathrm{bear1}} h_{\mathrm{bear1}} + F_{\mathrm{bear2}} h_{\mathrm{bear2}} = F_{\mathrm{ubw}} h_{\mathrm{ubw}} + F_{\mathrm{ro}} h_{\mathrm{ro}} + F_{\mathrm{lbw}} h_{\mathrm{lbw}}, \tag{13}$$

where $F_{\mathrm{ecc}} = m_{\mathrm{ecc}} e\omega^2$ and $h_{\mathrm{bear1,bear2,ubw,lbw,ro}}$ is the height shown in Fig. 2(b). From Equations (12) and (13), F_{bear1} and F_{bear2} are obtained. $\boldsymbol{F}_{\mathrm{cyl}}(\theta) = \left(F_{x_{\mathrm{cyl}}}, F_{y_{\mathrm{cyl}}}, F_{z_{\mathrm{cyl}}}\right)^{\mathrm{T}}$ caused by $F_{\mathrm{bear}i}$ $(i = 1, 2)$ is expressed as

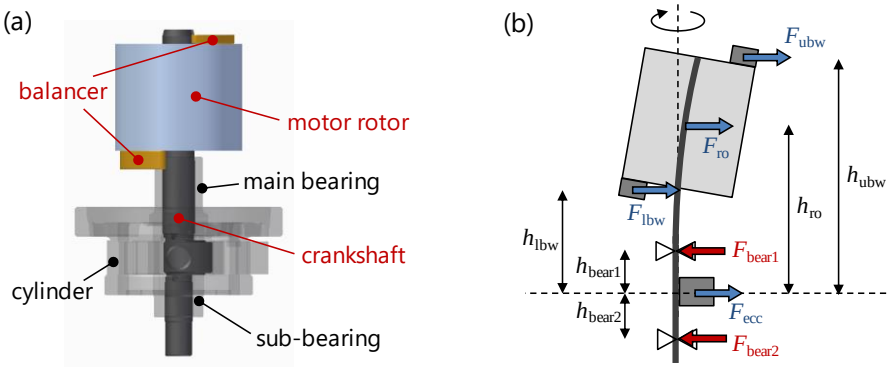

Figure 2: Schematic drawings of (a) rotor system and (b) model for formulating deflection of crankshaft and centrifugal forces

$\boldsymbol{F}_{\text{cyl}}(\theta) = (F_{\text{bear}i}\sin\theta\,, F_{\text{bear}i}\cos\theta\,, 0)^{\text{T}}$. $\boldsymbol{F}(\theta)$ and $\boldsymbol{T}(\theta)$ caused by $F_{\text{bear}i}$ are then obtained with Equations (7) and (8). $\boldsymbol{F}(\theta)$ and $\boldsymbol{T}(\theta)$ for a twin-cylinder type can be formulated in the same way as those of a single-cylinder type, except that the contribution of the centrifugal force of another eccentric part of the crankshaft is added to Equations (12) and (13).

2.3 Inertial Force of the Piston

Swing motion of the piston is a phenomenon which only exists in a swing compressor, not in a rotary compressor. The swing motion of the piston causes an inertial force, which is one of the excitation forces for rigid-body vibration. The swing motion can be categorized into two types of motion: one is the reciprocating motion in the blade direction and the other is the pendular motion in the swing angle direction, as shown in Fig. 3 (a). The excitation force caused by each motion is formulated in this subsection.

The inertial force caused by the reciprocating motion $F_{\text{iner\_BL}}(\theta)$ is applied to the crankshaft and it excites the vibration of the compressor via its bearings. $F_{\text{iner\_BL}}(\theta)$ is calculated as

$$F_{\text{iner\_BL}}(\theta) = m_{\text{pis}}\frac{\mathrm{d}^2 L_{\text{b}}}{\mathrm{d}t^2}\cos(\pi-\theta-\varphi), \tag{15}$$

where L_{b} is the length shown in Fig 3(b) and φ is the swing angle, which are expressed as

$$\begin{aligned} L_{\text{b}} &= \sqrt{e^2+L^2-2eL\cos\theta} - r - (L-R) \cong e\left(1-\cos\theta-\frac{e}{4L}\cos 2\theta\right), \\ \varphi &\cong \sin\varphi = \frac{e\sin\theta}{\sqrt{e^2+L^2-2eL\cos\theta}} \cong \frac{e}{L}\sin\theta + \frac{1}{2}\left(\frac{e}{L}\right)^2\sin 2\theta + \frac{27}{8}\left(\frac{e}{L}\right)^3\sin 3\theta. \end{aligned} \tag{16}$$

$\boldsymbol{F}_{\text{cyl}}(\theta)$ caused by $F_{\text{iner}_{\text{BL}}}(\theta)$ is expressed as $\boldsymbol{F}_{\text{cyl}}(\theta) = \left(F_{\text{iner\_BL}}\sin\theta\,, F_{\text{iner\_BL}}\cos\theta\,, 0\right)^{\text{T}}$. $\boldsymbol{F}(\theta)$ and $\boldsymbol{T}(\theta)$ caused by $F_{\text{iner\_BL}}(\theta)$ are then obtained with Equations (7) and (8).

The inertial force caused by the pendular motion $F_{\text{iner\_phi}}(\theta)$ is applied to the swing bush and it excites the vibration of the compressor via its cylinder. $\boldsymbol{F}(\theta)$ and $\boldsymbol{T}(\theta)$ caused by $F_{\text{iner\_phi}}(\theta)$ are calculated in the same way as those caused by $F_{\text{iner\_BL}}(\theta)$. $F_{\text{iner\_phi}}(\theta)$ is expressed as

$$F_{\text{iner\_phi}}(\theta) = -\frac{I_{\text{pis}}\ddot{\varphi}}{\sqrt{e^2+L^2-2eL\cos\theta}} \cong \frac{I_{\text{pis}}e\omega^2}{L^2}\left[\sin\theta + \frac{5e}{2L}\sin 2\theta + \frac{19}{4}\left(\frac{e}{L}\right)^2\sin 3\theta\right]. \tag{17}$$

$\boldsymbol{F}_{\text{cyl}}(\theta)$ is calculated as $\boldsymbol{F}_{\text{cyl}}(\theta) = \left(-F_{\text{iner\_phi}}\cos\varphi\,, -F_{\text{iner\_phi}}\sin\varphi\,, 0\right)^{\text{T}}$, and then $\boldsymbol{F}(\theta)$ and $\boldsymbol{T}(\theta)$ are obtained with Equations (7) and (8).

As for a twin-cylinder type swing compressor, you can formulate the inertial force caused by both the reciprocating motion and the pendular motion in the same way as described in the following. When the inertial force in one cylinder is expressed as $\boldsymbol{F}_{\text{cyl1}}(\theta)$, which is formulated as Equations (15) or (17), the force in the other cylinder $\boldsymbol{F}_{\text{cyl2}}(\theta)$ is expressed as $\boldsymbol{F}_{\text{cyl2}}(\theta) = \boldsymbol{F}_{\text{cyl1}}(\theta+\pi)$. The total inertial force $\boldsymbol{F}_{\text{cyl\_total}}(\theta)$ is expressed as $\boldsymbol{F}_{\text{cyl\_total}}(\theta) = \boldsymbol{F}_{\text{cyl1}}(\theta) + \boldsymbol{F}_{\text{cyl2}}(\theta)$, and then $\boldsymbol{F}(\theta)$ and $\boldsymbol{T}(\theta)$ are obtained with Equations (7) and (8).

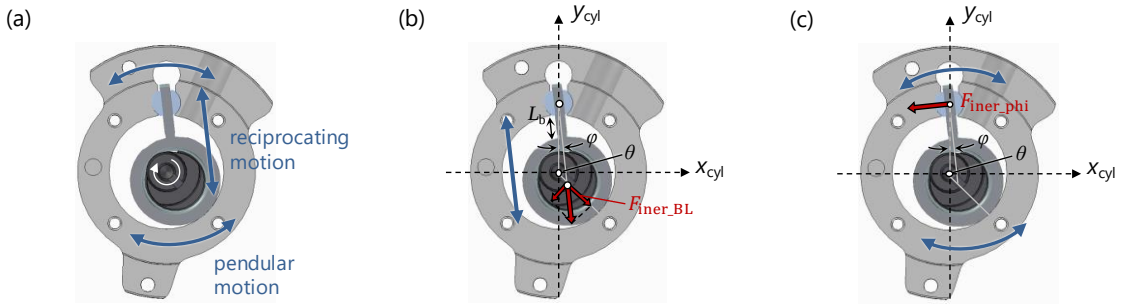

Figure 3: Schematic drawings of (a) swing motion of piston, (b) inertial force caused by reciprocating motion in the blade direction and (c) inertial force caused by pendular motion in the swing angle direction.

2.4 Compression Torque

As shown in Fig. 4 (a), torque caused by the pressure difference between the compression chamber and the suction chamber is applied to the rotor system. The reaction torque, which we call the compression torque, then excites the rigid-body vibration of the compressor. The compression torque has the only component of around z axis $T_{\mathrm{comp}\_z}(\theta)$, which is expressed as

$$T_{\mathrm{comp}\_z}(\theta) = -\Delta P(\theta) V_{SL}(\theta), \tag{18}$$

where $\Delta P(\theta)$ is the pressure difference between the compression chamber and the suction chamber, and $V_{SL}(\theta)$ the product of the area at which $\Delta P(\theta)$ applies and the arm length of the compression torque. When both $\Delta P(\theta)$ and $V_{SL}(\theta)$ are formulated in a Fourier series representation, $T_{\mathrm{comp}\_z}(\theta)$ is also expressed in the representation. In this sub-section, the Fourier series representations of $\Delta P(\theta)$ and $V_{SL}(\theta)$ are formulated.

From the Poisson's law for adiabatic process in thermodynamics, the pressure of the compression chamber at a crank angle θ is expressed as

$$P_{\mathrm{c}}(\theta) = \begin{cases} P_{\mathrm{s}} \left(\dfrac{V_{\mathrm{cc}}}{V_{\mathrm{c}}(\theta)} \right)^{\gamma} & (0 \le \theta \le \theta_{\mathrm{d}}) \\ P_{\mathrm{d}} & (\theta_{\mathrm{d}} \le \theta \le 2\pi) \end{cases} \tag{19}$$

where $V_{\mathrm{c}}(\theta)$ is geometrically obtained as follows:

$$V_{\mathrm{c}}(\theta) \cong \frac{eH}{2} \left[(R+r)(2\pi - \theta) + \left(R + \frac{r^2}{L} \right) \sin\theta - d(1 - \cos\theta) \right]. \tag{20}$$

You can obtain the Fourier coefficients of $P_{\mathrm{c}}(\theta)$ numerically by performing FFT. If you want to obtain the Fourier coefficients without FFT, they can be obtained by the calculation based on the definition of the Fourier coefficients: that is, by calculating the inner product of $P_{\mathrm{c}}(\theta)$ and trigonometric functions. However, Equation (19) is too complex to calculate the inner product. In this study, to make the calculation of the inner product easier, $P_{\mathrm{s}}(V_{\mathrm{cc}}/V_{\mathrm{c}}(\theta))^{\gamma}$ was approximated with a quartic function as $P_{\mathrm{s}}(V_{\mathrm{cc}}/V_{\mathrm{c}}(\theta))^{\gamma} \cong A\theta^4 + B\theta^3 + C\theta^2 + D\theta + E$, where A, B, C, D and E were the coefficients. These coefficients can be formulated by the boundary conditions at $\theta = 0$, $\pi/2$ and π. This approximated function was in good agreement with the original function, as shown in Fig. 4 (b). Once $P_{\mathrm{c}}(\theta)$ is expressed by using a polynomial function, the inner product with trigonometric functions can easily be calculated.

$V_{\mathrm{SL}}(\theta)$ can be geometrically obtained. The detail process of the calculation is omitted in this paper, but it is expressed as

$$V_{SL}(\theta) \cong \frac{1}{2} eH \left\{ R + r - \left[2R - \frac{e(R+r)}{L} \right] \cos\theta + e \left(1 - \frac{3R+r}{2L} \right) \cos 2\theta \right\}. \tag{21}$$

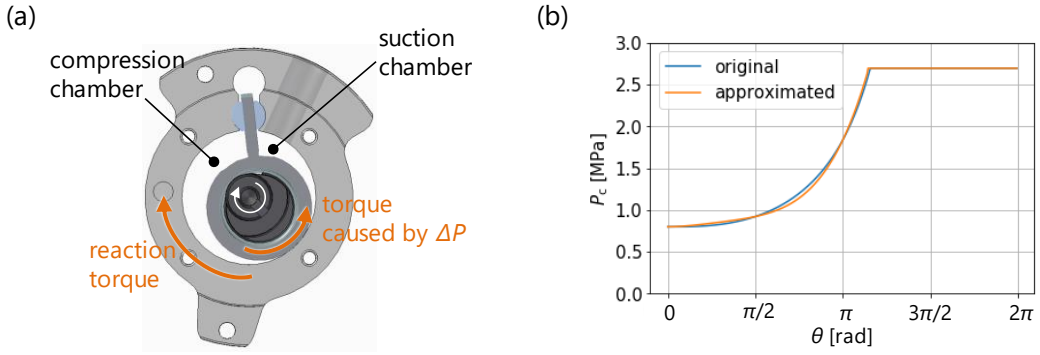

Figure 4: (a) Schematic drawing of compression torque. (b) An example of the comparison between original $P_{\mathrm{c}}(\theta)$ and approximated $P_{\mathrm{c}}(\theta)$.

3. Method

We performed theoretical calculations and experimental measurements for vibration of typical swing compressors listed in Table 1. The conditions for the calculations and experiments of each compressor are also presented in Table 1. Calculations were performed with the theoretical equations presented in the previous section. The experiments were performed on the equipment with the flexibly supporting system developed in the previous study (Wada *et al*., 2016). The vibration of each compressor listed in Table 1 was measured with a triaxial acceleration sensor attached to the compressor as shown in Fig. 5. The radial and tangential vibrations measured by the sensor were compared with the calculated vibrations.

We carried out detailed theoretical analysis on compressors No. 1 and No. 3. The amplitude and the phase of the vibration caused by each excitation force were calculated separately. The contribution of each excitation force to the vibration was then analyzed.

Table 1: Conditions for the calculations and experiments.

Compressor No.	Type	Condensation Temperature	Evaporation Temperature	Rotational Speed	Refrigerant
1	single cylinder	45 °C	−7 °C	32 - 116 rps	R32
2	single cylinder	55 °C	10 °C	52 - 100 rps	R32
3	twin cylinder	45 °C	−7 °C	32 - 116 rps	R32
4	twin cylinder	45 °C	−5 °C	42 - 118 rps	R32

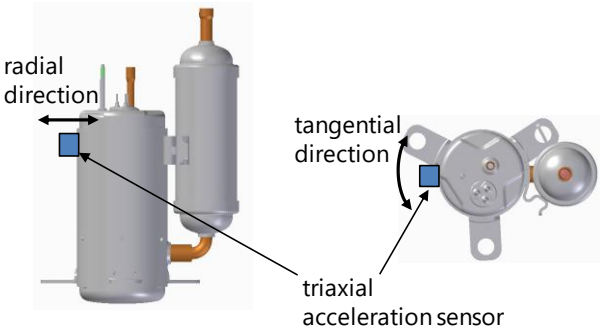

Figure 5: Schematic drawing of the position of the triaxial acceleration sensor.

4. RESULTS AND DISCUSSION

Firstly, Fig. 6 shows the comparison between calculated and measured vibrations. The calculated vibration was in good agreement with the measured one for both 1*n* and 2*n* vibrations of each compressor. This result indicates the validity of the theoretical calculations of the vibrations for both single- and twin-cylinder types of swing compressors.

In the following, we show the results of the theoretical analysis of the contribution of each excitation force for 1*n* and 2*n* vibrations. Figs. 7 - 9 show the results of the detailed analysis of the 1*n* vibration of compressor No. 1, the 1*n* vibration of compressor No. 3, and the 2*n* vibration of compressor No. 1, respectively. The contribution of each excitation force is shown in each figure. (a) and (b) of each figure show the radial vibration, whereas (c) and (d) show the tangential vibration. Also, (a) and (c) of each figure shows the amplitude and phase of the vibration generated by each excitation force at the rotational speed of 100 rps, whereas (b) and (d) of each figure shows the dependence on N of the magnitude of the vibration caused by each excitation force. Here, since the results of the analysis on compressors No. 1 and No. 3 show the typical vibration properties of single- and twin-cylinder type, we call compressors No. 1 and No. 3 simply 1YC (single-cylinder type swing compressor) and 2YC (twin-cylinder type swing compressor). Furthermore, for simplicity of description, we call the centrifugal force of the rotor system, the inertial force caused by the reciprocating motion, the inertial force caused by the pendular motion, and the compression torque F_{rotor}, $F_{\mathrm{pis\_BL}}$, $F_{\mathrm{pis\_phi}}$ and F_{comp}.

As shown in Fig 7 (a) and (b), the radial 1*n* vibration of 1YC is contributed by F_{rotor}, $F_{\mathrm{pis\_BL}}$ and $F_{\mathrm{pis\_phi}}$. The amplitude of the vibration caused by $F_{\mathrm{pis\_phi}}$ is small compared to that by F_{rotor} and $F_{\mathrm{pis\_BL}}$ because the direction

of $F_{\text{pis\_phi}}$ is almost orthogonal to the radial direction as shown in Fig. 3 (c). It should be noted that the vibrations by F_{rotor} and $F_{\text{pis\_BL}}$ are almost in opposite phase with each other, and the amplitudes are almost the same. This relationship between F_{rotor} and $F_{\text{pis\_BL}}$ results in the totally small radial 1n vibration of 1YC, in spite of the large amplitudes of the vibrations by F_{rotor} and $F_{\text{pis\_BL}}$. That is due to the design of balancers. $F_{\text{pis\_BL}}$ includes the centrifugal force applied to the cylindrical part of the piston. The balancers are designed so that the centrifugal force of the rotor system and the force of the cylindrical part of the piston are balanced. As shown in Fig. 7 (b), and also formulated in Sec. 2, F_{rotor}, $F_{\text{pis\_BL}}$ and $F_{\text{pis\_phi}}$ increase in proportion to N^2. Nevertheless, the radial 1n vibration of 1YC stays small as long as these excitation forces are balanced.

The tangential 1n vibration of 1YC has a completely different property from that of the radial one. In addition to the contribution of F_{rotor}, $F_{\text{pis\_BL}}$ and $F_{\text{pis\_phi}}$, the tangential 1n vibration of 1YC is largely contributed by F_{comp}. Although F_{rotor}, $F_{\text{pis\_BL}}$ and $F_{\text{pis\_phi}}$ are proportional to N^2, F_{comp} is constant regardless of N, resulting in the large tangential 1n vibration of 1YC at any N. Moreover, unlike in the case of the radial 1n vibration of 1YC, F_{rotor}, $F_{\text{pis\_BL}}$ and $F_{\text{pis\_phi}}$ are not balanced in the tangential one. As a result, the total tangential 1n vibration of 1YC increases with N, in addition to the constantly large vibration caused by F_{comp}. The large tangential 1n vibration of single-cylinder type rotary compressor, including 1YC, often becomes a problem in the development of the compressor. The results shown in this study indicates that there are two types of solutions for the problem: one is to reduce the amplitude of each excitation force, and the other is to balance the excitation forces with each other.

The radial 1n vibration of 2YC has the same property as that of 1YC, except for the smaller amplitudes of the vibrations by F_{rotor}, $F_{\text{pis\_BL}}$ and $F_{\text{pis\_phi}}$ in 2YC compared to those in 1YC. 2YC has two eccentric parts in the crankshaft. The centrifugal forces applied to the eccentric parts generally have the same magnitudes and are in opposite directions with each other, resulting in the more balanced, that is, the smaller F_{rotor} of 2YC compared to that of 1YC. The same explanation can be applied to $F_{\text{pis\_BL}}$ and $F_{\text{pis\_phi}}$. The one piston moves in the opposite phase with the other piston, resulting in the smaller $F_{\text{pis\_BL}}$ and $F_{\text{pis\_phi}}$. It is important that the total 1n vibration of 2YC is almost the same with that of 1YC although the amplitudes of the vibrations by F_{rotor}, $F_{\text{pis\_BL}}$ and $F_{\text{pis\_phi}}$ of 2YC are quite different to those of 1YC. This result indicates that the small total vibration does not necessarily require that the amplitudes of the excitation forces be small. Even though the excitation forces have large amplitude, the total vibration becomes small if these excitation forces are balanced with each other.

The property of the tangential 1n vibration of 2YC is not similar to that of 1YC. Whereas the tangential 1n vibration of 1YC has the large contribution of F_{comp}, the vibration of 2YC has no contribution of F_{comp}. 2YC has two cylinders and the compression of the refrigerant in one cylinder is performed in the opposite phase with that in the other cylinder. Therefore, the compression torque in one cylinder cancels out that in the other cylinder, resulting in no contribution of F_{comp} to the tangential 1n vibration of 2YC. As a result, the property of the tangential 1n vibration of 2YC is similar to that of the radial 1n vibration of 2YC, except for having a bit larger contribution of $F_{\text{pis\_phi}}$.

As for the 2n vibration, 1YC and 2YC have the same property. The results of the analysis on 2n vibration described below are then applied to both for 1YC and 2YC. A characteristic of 2n vibration, which is different from 1n vibration, is that F_{rotor} does not contribute to both radial and tangential 2n vibrations. This indicates that the balancers cannot be designed for the reduction of 2n vibration. The excitation forces which contribute to 2n vibration are $F_{\text{pis\_BL}}$, $F_{\text{pis\_phi}}$ and F_{comp}. $F_{\text{pis\_BL}}$ and $F_{\text{pis\_phi}}$ contribute to both radial and tangential 2n vibration, and F_{comp} contributes to only the tangential 2n vibration. The radial 2n vibration is very small and does not have any notable property, whereas the tangential 2n vibration has an interesting property. As shown in Fig. 9 (c), the phase of the tangential 2n vibration caused by F_{comp} is almost opposite to that caused by $F_{\text{pis\_phi}}$, meaning that the vibrations caused by F_{comp} are canceled out by $F_{\text{pis\_phi}}$. These excitation forces have different dependence on N: F_{comp} is constant regardless of N, whereas $F_{\text{pis\_phi}}$ increases in proportion to N^2. Therefore, the canceling effect becomes larger with the increase of N. As a result, the total tangential 2n vibration decreases with the increase of N, as shown in Fig. 9 (d). This canceling phenomenon is owing to $F_{\text{pis\_phi}}$, which does not exist in rotary compressors. It means that this vibration property is one of the distinct properties of swing compressors and is not observed in rotary compressors.

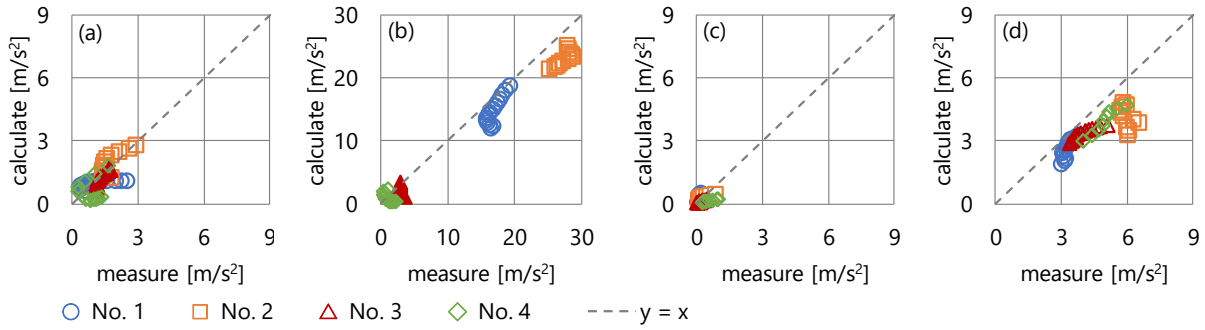

Figure 6: Comparison between the measured vibration and calculated vibration. (a) Radial 1*n* vibration. (b) Tangential 1*n* vibration. (c) Radial 2*n* vibration. (d) Tangential 2*n* vibration.

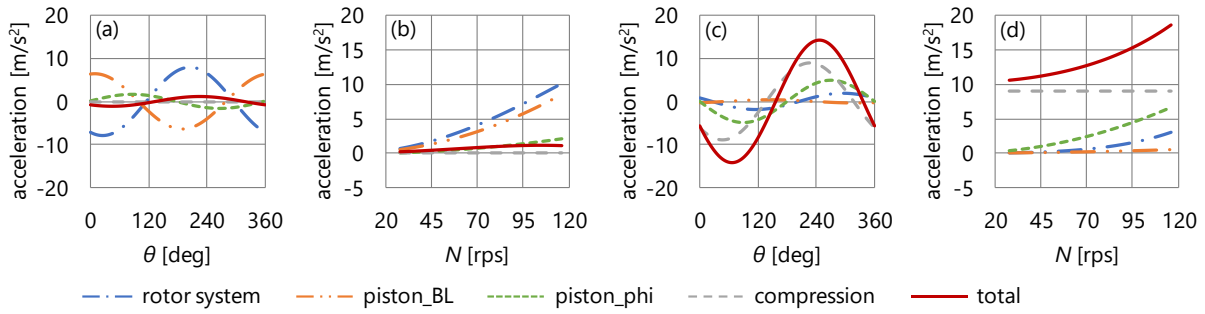

Figure 7: Contribution of each excitation force to 1*n* vibration of 1YC. (a) Amplitude and phase of the radial 1*n* vibration caused by each excitation force at 100 rps. (b) Dependence on *N* of magnitude of the radial 1*n* vibration caused by each excitation force. (c) Same as (a), but for the tangential 1*n* vibration. (d) Same as (b), but for the tangential 1*n* vibration.

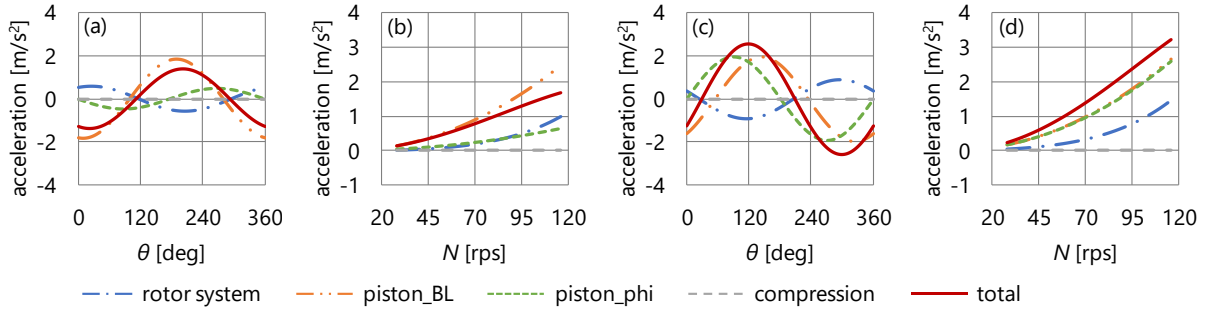

Figure 8: Same as Figure 7, but for 1*n* vibration of 2YC.

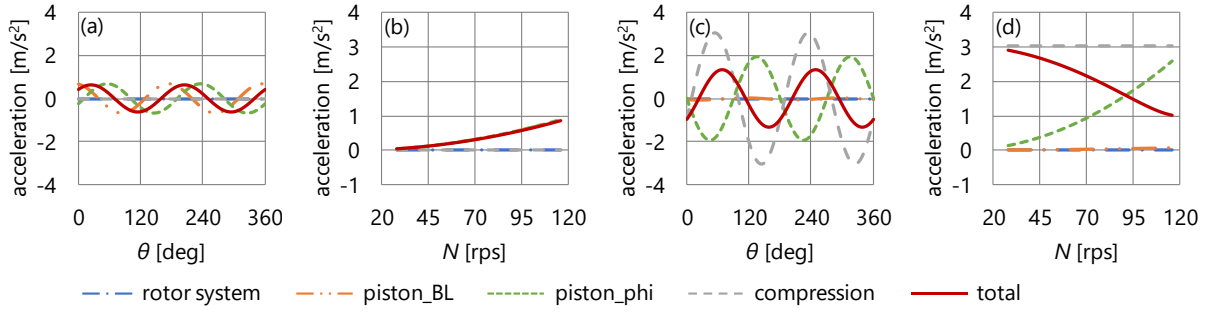

Figure 9: Same as Figure 7, but for 2*n* vibration of 1YC.

5. CONCLUSIONS

This study performed a theoretical analysis of rigid-body vibration in a swing compressor. Firstly, we classified the main factors of the vibration into three type of excitation forces and formulated the vibration caused by each excitation force. Secondly, the rigid-body vibrations of typical swing compressors were measured. The calculated vibrations were confirmed to be consistent with the measured ones. Thirdly, the theoretical analysis of the properties of rigid-body vibrations of both single- and twin-cylinder type swing compressors were performed. The primary and secondary components in the frequency domain of the radial and tangential vibrations were theoretically analyzed from the viewpoint of the contribution of each excitation force. To our knowledge, this is the first time to perform the following:

- Both the amplitude and the phase of the primary and secondary components of the vibration caused by each excitation force in the frequency domain were formulated separately without any other numerical calculation technique, including FFT.
- The contribution of each excitation force to vibration, including the relationship of the phase of each excitation force, was analyzed.

The results of the theoretical analysis clearly indicated that not only was simply reducing the magnitudes of the excitation forces effective but balancing the excitation forces was also very effective for the reduction of the vibration. Balancing the excitation forces is more advanced than reducing the magnitudes of the excitation forces because both amplitude and phase of each excitation force must be obtained to balance the excitation forces. This study theoretically formulated both amplitude and phase of the excitation forces which are the main causes of vibrations, and the validity of the theoretically-calculated vibration is confirmed by a comparison to a measured one. We expect that this study will help the development of a more advanced technique for the reduction of the vibration in a theoretical viewpoint.

NOMENCLATURE

e	eccentricity of piston center
H	cylinder height
I_{pis}	moment of inertia of piston
L	length between center of cylinder and center of swing bushes
$m_{\mathrm{ubw/lbw/ro}}$	mass of upper balancer/lower balancer/motor rotor
m_{ecc}	mass of eccentric part of crankshaft
m_{pis}	mass of piston
P_{c}	pressure of compression chamber
P_{d}	discharge pressure
P_{s}	suction pressure
R	inner radius of cylinder
r	outer radius of piston
$r_{\mathrm{ubw/lbw}}$	distance between center axis of motor rotor and center of gravity of upper/lower balancer
V_{cc}	cylinder volume
V_{c}	volume of compression chamber
γ	polytropic index
θ	rotating angle of crankshaft
θ_{d}	rotating angle of crankshaft at which P_{c} reaches P_{d}

REFERENCES

Huang, J *et al*. (2010). Dynamic Balance Technology of Inverter Controller Rotary Compressor. *Proceedings of the International Compressor Engineering Conference at Purdue* (Paper 1140).

Imaichi, K. *et al*. (1982). Vibration Analysis of Rotary Compressor. *Proceedings of the International Compressor Engineering Conference at Purdue* (Paper 407).

Wada, H. *et al*. (2016). Vertical-Vibration Suppressing Design of Accumulator with New Vibration-Measuring Method. *Proceedings of the International Compressor Engineering Conference at Purdue* (Paper 1158).

Zhang, H. *et al*. (2014). Dynamic behaviors of the crankshafts in single-cylinder and twin-cylinder rotary compressors. *International Journal of Refrigeration*, 47, 36-45.